Large Rashba spin-orbit coupling and high-temperature quantum anomalous Hall effect in Re-intercalated graphene/CrI$_3$ heterostructure

Yulei Han [1,2,3,*] Zhi Yan [1,2,4,*] Zeyu Li,[1,2] Xiaohong Xu,[4] Zhenyu Zhang,[1,5] Qian Niu,[2] and Zhenhua Qiao [1,2,5,†]

[1]*International Center for Quantum Design of Functional Materials,*
University of Science and Technology of China, Hefei, Anhui 230026, China
[2]*CAS Key Laboratory of Strongly-Coupled Quantum Matter Physics, and Department of Physics,*
University of Science and Technology of China, Hefei, Anhui 230026, China
[3]*Department of Physics, Fuzhou University, Fuzhou, Fujian 350108, China*
[4]*School of Chemistry and Materials Science & Key Laboratory of Magnetic Molecules and Magnetic Information Materials of Ministry*
of Education & Research Institute Materials Science, Shanxi Normal University, Taiyuan 030031, China
[5]*Hefei National Laboratory, University of Science and Technology of China, Hefei 230088, China*

In 2010, the quantum anomalous Hall effect (QAHE) in graphene was proposed in the presence of Rashba spin-orbit coupling and a ferromagnetic exchange field. After a decade of experimental exploration, the anomalous Hall conductance can only reach about 0.25 in units of $2e^2/h$, which was attributed to the tiny Rashba spin-orbit coupling. Here, we show theoretically that Re-intercalation in a graphene/CrI$_3$ heterostructure can not only induce sizable Rashba spin-orbit coupling (>40 meV), but also open up large band gaps at valleys K (22.2 meV) and K' (30.3 meV), and a global band gap over 5.5 meV (19.5 meV with random Re distribution) hosting QAHE. A low-energy continuum model is constructed to explain the underlying physical mechanism. We find that Rashba spin-orbit coupling is robust against external stress whereas a tensile strain can increase the global bulk gap. Furthermore, we comprehensively explore the electronic properties of $3d$, $4d$, $5d$ transition-metal intercalation in graphene/CrI$_3$ systems.

I. INTRODUCTION

The quantum anomalous Hall effect (QAHE) is the quantized version of the anomalous Hall effect without requiring an external magnetic field [1–3] and is significant in both fundamental physics and potential applications for low-power electronics. In the last decade, QAHE was mainly proposed in materials with Dirac-like dispersion, e.g., $\mathbb{Z}_2$ topological insulator thin films and graphene systems. It is known that the interplay between spin-orbit coupling (SOC) and ferromagnetism is crucial for the QAHE realization [4,5]. On one side, topological insulators naturally possess considerable SOC, thus one only needs to introduce the ferromagnetism to realize QAHE. Three years after the first theoretical proposal in 2010, $\mathbb{Z}_2$ topological insulator-based QAHE was experimentally observed in magnetically doped topological insulators at the temperature of 30 mK [6], and recently the QAHE observation temperature has been raised up to 6.5 K [7].

On the other side, although the graphene-based QAHE was also proposed in 2010 by introducing Rashba SOC and ferromagnetism [5], so far the experimentally observed anomalous Hall conductance can only reach up to 25% of $2e^2/h$ by coupling graphene with Y$_3$Fe$_5$O$_{12}$ magnetic thin film [8,9]. It was shown that atomic doping is most effective in inducing Rashba SOC and ferromagnetism due to the chemical bonding between $3d$-orbitals of adatoms and the π orbital of graphene [5,10,11]. However, the magnetic adatoms tend to form clusters due to the atomic migration. Later, we found that the magnetic insulating substrate can form a stable heterostructure with graphene [12], which can open up a band gap to host QAHE [13–16]. Its major obstacle is the tiny band gap ($\approx$1 meV) from the weak Rashba SOC that is determined by the physical van der Waals interaction between magnetic insulator and graphene [8,9,17,18]. Thus, pursuing large Rashba SOC becomes crucial for the observation of QAHE in graphene.

By integrating the above two strategies, element intercalation becomes an ideal choice. So far, there have been various intercalated graphene systems that were proposed in exploring Kane–Mele-type $\mathbb{Z}_2$ topological insulators or large Rashba effects in metallic substrates [19–29]. Inspired by these findings and recently observed two-dimensional ferromagnetic materials (e.g., CrI$_3$) [30–33], in this Letter, we provide a systematic study on $5d$-intercalated graphene/CrI$_3$ systems. We find that the large Rashba SOC over 40 meV can be induced, and a sizable topological band gap opens up to host the QAHE with a Chern number of $\mathcal{C} = -2$. We implement an effective model to clearly understand the effects from exchange field, intrinsic and Rashba SOC in the formation of QAHE. By applying external stress, we further show that the Rashba gap is robust whereas a tensile strain can even enhance the bulk band gap. A comprehensive study of electronic properties

---

*These authors contributed equally to this work.
†Corresponding author: qiao@ustc.edu.cn
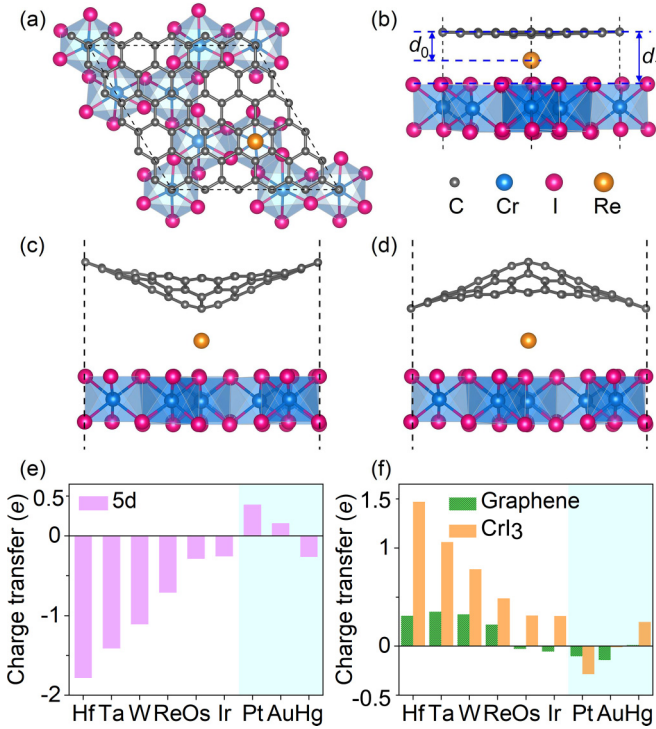
FIG. 1. (a) Top and (b) side views of the Re-intercalated graphene/CrI_3 heterostructure. d_0 represents the average distance between Re atom and the surrounded six carbon atoms, and d_1 represents the average distance between graphene and CrI_3. Schematic plot of $5d$-intercalation-induced (c) attractive and (d) repulsive interaction between $5d$ atom and graphene. Charge transfer for (e) $5d$ atom and (f) graphene/CrI_3 in the intercalated systems.

of $3d$, $4d$, $5d$ transition-metal intercalation in graphene/CrI_3 systems is conducted. Our findings provide a solid strategy to engineer large Rashba SOC and therefore open a sizable band gap to harbor QAHE, as well as provide a concrete recipe for the experimental realization of QAHE in graphene.

II. SYSTEM MODELS AND CALCULATION METHODS

Our first-principles calculations are performed by using the projected augmented-wave method [34] as implemented in the Vienna *ab initio* simulation package (VASP) [35,36] and the detailed parameters are described in the Supplemental Material [37]. We first investigate the stable intercalation site of $5d$ atoms and take Re as an example. Four different heterostructure configurations, i.e., C(H)-Re-Cr(T), C(T)-Re-Cr(T), C(T)-Re, and C(T)-Re-I(H) are constructed, with H and T respectively representing "hollow" and "top" sites [see Figs. 1(a) and 1(b) for the first configuration and Fig. S1 for other three configurations] [37]. We find that C(H)-Re-Cr(T) is the most stable geometry for Re intercalation from the total-energy calculations as summarized in Table S1 [37]. Table I summarizes the atomic distances d_0 and d_1 of $5d$-intercalated graphene/CrI_3 heterostructure as defined in Fig. 1(b). One can see that d_0 and d_1 for Re-intercalated system are respectively 1.78 and 3.59 Å, and also are the shortest among all $5d$-intercalated system, indicating the strongest Re-mediated van der Waals interaction between graphene and CrI_3. The

TABLE I. Atomic distance of $5d$-intercalated graphene/CrI_3 heterostructure. The most stable geometry of C(H)-X-Cr(T) is used. The last row denotes the attractive $(+)$ /repulsive $(-)$ interaction between graphene and $5d$ atoms.

$X =$	Hf	Ta	W	Re	Os	Ir	Pt	Au	Hg
d_0	2.15	1.98	1.88	1.78	2.22	1.89	3.61	3.52	3.86
d_1	3.66	3.61	3.59	3.59	3.69	3.65	3.70	3.70	3.69
Interaction	$+$	$+$	$+$	$+$	$+$	$+$	$-$	$-$	$-$

inclusion of intercalated atoms may induce the attractive or repulsive interaction, as schematically displayed in Figs. 1(c) and 1(d). By analyzing the relative positions of the surrounding carbon atoms, we find an attractive interaction between $5d$ atom and graphene for Hf-Ir, whereas a repulsive interaction for Pt, Au, Hg (see Table I and Fig. S2). This can be qualitatively understood by the charge transfer process as demonstrated in Figs. 1(e) and 1(f), with a sign change from Ir to Pt for $5d$ atoms and CrI_3. Hereinafter, we focus on exploring the electronic properties of a concrete Re-intercalated graphene/CrI_3 heterostructure.

III. BAND STRUCTURES

We start by analyzing the band structures. Figures 2(a) and 2(c) display the spin-resolved bands, with C-p_z orbital contribution highlighted in green. One can find large spin splitting of ≈ 300 meV (94 meV) in conduction (valence) bands, and can also observe that the Re intercalation greatly enhances the exchange interaction between CrI_3 and graphene from spin-density distribution [see Figs. S3(a) and S3(b)] [37]. The crossing of spin-up and -down bands indicates a possible band-gap opening if SOC is introduced as proposed [5]. The estimated Curie temperature from Monte Carlo simulations is 95 K (see Fig. S4) [37]. The remarkable increase of the Curie temperature from Re intercalation in graphene/CrI_3 heterostructure makes it a promising platform to realize high-temperature QAHE.

As displayed in Figs. 2(b) and 2(d), the inclusion of spin-orbit coupling opens sizable local band gaps of 22.2 and 30.3 meV at valleys K and K', respectively. It is noteworthy that the local band gaps are not aligned, indicating the potential presence of other physical ingredients, e.g., the sublattice staggered potential or intrinsic SOC. Even so, a considerable global band gap around 5.5 meV still exists, which is about five times larger than our previous theoretical predictions in graphene/$BiFeO_3$ systems [12]. By analyzing different atomic orbitals (see Fig. S5) [37], one can see that Cr-(d_{xy}, $d_{x^2-y^2}$, d_{yz}, d_{xz}), I-p, C-p_z and Re-d_{z^2} orbitals are strongly hybridized near the global gap. The inclusion of the Re atom hybridizes the C-p_z and I-p orbitals via Re-d_{z^2} orbital, enhancing the exchange interaction and Rashba SOC. This can also be verified from charge transfer, i.e., Re atom transfers 0.22 (0.49) electrons to C (I), and the presence of Re intercalation changes the charge distribution dramatically and enhances the charge-density overlap between CrI_3 and graphene [see Figs. S3(c) and S3(d)]. Moreover, the Rashba SOC in graphene induced by the heavy metal element is determined by the hybridization between C-p and
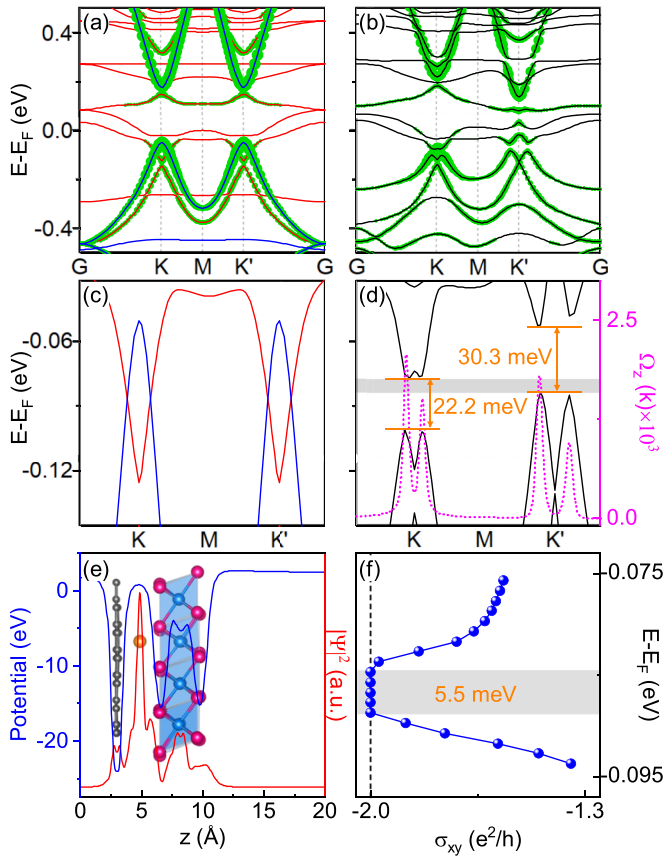
FIG. 2. Electronic band structures of Re-intercalated graphene/CrI₃ heterostructure (a) without SOC and (b) with SOC. Red and blue in panel (a) represent spin-up and spin-down states, respectively. Green circle represents states from C-p_z orbital. (c), (d) The corresponding zooming-in band structures near the band crossing point. In panel (d), the Berry curvature and the global band gap are shown by the pink dashed line and gray rectangle, respectively. (e) Planar-averaged distribution of potential and electron density $|\Psi(z)|^2$ along out-of-plane direction. The corresponding atomic positions are also superposed onto the curves. (f) Anomalous Hall conductance as a function of Fermi level, with σ_{xy} being quantized for energies inside the bulk gap.

$5d$-d orbital [25]. The strong p-d orbital hybridization in Re-intercalated graphene leads to a large Rashba SOC (see Fig. S10) [37]. The enhancement of Rashba SOC can also be qualitatively explained by the planar-averaged asymmetric potential and electron density distributions [see Fig. 2(e)], with the screening charge around the band crossing point primarily distributed around Re, implying the critical role of Re intercalation.

IV. TOPOLOGICAL PROPERTIES

Then, we study the topological properties of the Re-intercalated graphene/CrI₃ system. As shown in Fig. 2(d), one can observe that the Berry curvature exhibits large peaks around valleys K and K', but vanishes elsewhere, indicating the existence of nonzero Chern number $\mathcal{C}$, i.e., the formation of the QAHE. In Fig. 2(f), one see that the Hall conductance is quantized for a Fermi energy lying inside the band gap, i.e., $\sigma_{xy} = -2.0 \, e^2/h$.

The Re-intercalated graphene/CrI₃ system is distinct from the previously studied graphene/CrI₃ and $5d$-adsorbed graphene. In the previous graphene/CrI₃ heterostructure [14], the formation of QAHE with a small band gap requires a compressive strain to shift the Dirac cone of graphene to the gap of CrI₃. In contrast, the realization of QAHE in our Re-intercalated system does not require external stress and intrinsically has large Rashba SOC. In $5d$-adsorbed graphene, the strong hybridization between $d_{xz/yz}$ orbital and C-p_z orbital plays a crucial role in the formation of various topological phases [38,39]. To demonstrate the difference between Re-intercalated and Re-adsorbed systems, we compare the bands and density of states with and without CrI₃ in Re-intercalated graphene/CrI₃. As displayed in Fig. S6, in the absence of CrI₃, strong hybridization between C-p_z and Re-(s, $d_{xz/yz}$) orbitals is around the Fermi level whereas Re-d_{z^2} orbital is far away from the Fermi level, which is different from the density of states distribution in Re-intercalated graphene/CrI₃ [see Fig. S5] [37]. Therefore, one can find that the presence of CrI₃ significantly modifies the band structure of the heterostructure in two aspects, i.e., (i) the $d_{xz/yz}$ and d_{z^2} orbitals of Re are moved up and (ii) C-p_z orbital is strongly hybridized with d_{z^2} orbital, leading to a distinct physical origin of topological phases.

V. LOW-ENERGY CONTINUUM MODEL

The electronic states around valleys K/K' are dominated by p_z orbital of graphene. Therefore, one can construct an effective model Hamiltonian as below [5,12]:

$$H(\mathbf{k}) = v_F(\eta\sigma_x k_x + \sigma_y k_y)\mathbf{1}_S + \frac{\lambda_R}{2}(\eta\sigma_x s_y - \sigma_y s_x) + \eta\lambda_{SO}\sigma_z s_z + m_a\frac{\mathbf{1}_\sigma + \sigma_z}{2} + m_b\frac{\mathbf{1}_\sigma - \sigma_z}{2} + \delta\sigma_z\mathbf{1}_S, \tag{1}$$

where v_F is the Fermi velocity, $\eta = \pm 1$ labels the valley index, and σ and s are Pauli matrices for sublattice and spin degrees of freedom, respectively. The first term represents electron's hopping of pristine graphene, the second and third terms are respectively Rashba and intrinsic SOCs. The fourth and fifth terms describe the sublattice-dependent magnetic exchange fields, and the last term is the staggered sublattice potential. By fitting the first-principles band structure without and with

SOC, one can extract the effective system parameters, i.e., $m_a = 150$ meV, $m_b = 47$ meV, $\delta = 31$ meV, $\lambda_{SO} = 39$ meV, and $\lambda_R = 45$ meV.

Let us now analyze the influence of each physical ingredient on the band structure. As displayed in Fig. 3(a), the presence of unequal exchange field in different sublattices leads to a different spin splitting of conduction and valence bands, whereas the two valleys are identical
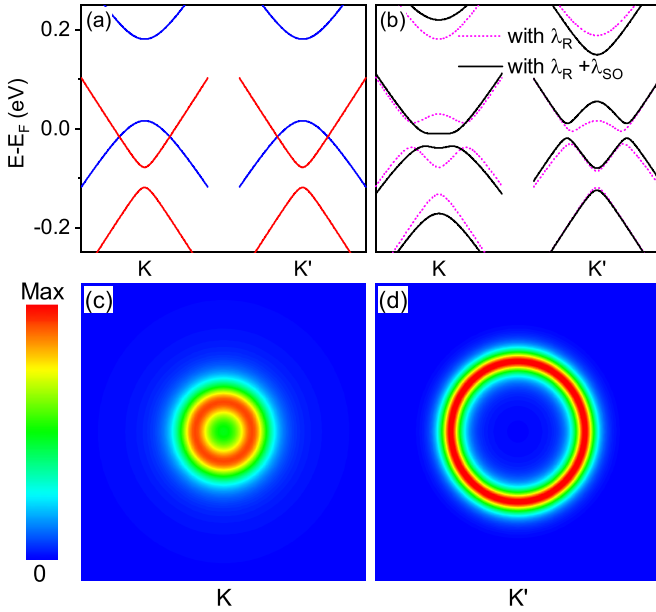
FIG. 3. Band structures from effective model (a) without SOC and (b) with SOC. The red (blue) color in panel (a) denotes a spin-up (spin-down) state. The pink dotted line in panel (b) indicates that only Rashba SOC is included whereas the black line indicates that both Rashba and Kane-Mele SOCs are considered. The corresponding Berry curvature distributions around (c) K and (d) K' points with SOC.

FIG. 4. (a) Band gaps of Re-intercalated graphene/CrI$_3$ as a function of out-of-plane strain. (b) The global gaps from the first-principles calculations and from the effective model in the absence of staggered sublattice potential, and the fitted Rashba SOC strength λ_R for graphene/CrI$_3$ intercalated with Cr, Nb, Ir, Re.

without SOC. It is noteworthy that the unequal exchange field is consistent with the spin density as displayed in Figs. S3(a) and S3(b), where visible spin polarization only exists at one graphene sublattice. When Rashba SOC is further considered [see Fig. 3(b), pink dotted line], one can observe that band gaps are opened at the band crossing points at each valley, and the local gaps at K and K' valleys become different due to the presence of staggered sublattice potential. In this case, the global band gap is only determined by the local gap of valley K'. However, from Fig. 2(d), one can observe that global band gap is determined by conduction band of valley K and valence band of valley K'. To well capture this character, the intrinsic SOC λ_{SO} should be further included in the effective model. As displayed in Fig. 3(b) (black line), the band structure with the four essential physical ingredients reproduces the low-energy physics of the first-principles results.

Figures 3(c) and 3(d) display the Berry curvature distributions around valley K and K', respectively. The sum over of Berry curvature in each valley gives $\mathcal{C}_{K/K'} = 1$, resulting in Chern number of $\mathcal{C} = \mathcal{C}_K + \mathcal{C}_{K'} = 2$. It is noteworthy that the Berry curvature distributions are different at two valleys, i.e., the Berry curvature peaks are close to valley K but are far away from valley K', which is also consistent with the Berry curvature from first-principles method [see Fig. 2(d)]. Remarkably, the large Rashba SOC strength, i.e., $\lambda_R = 45$ meV, in our intercalated system is about 30 times larger than that reported in the previous study [12], and the sizable Rashba SOC solves a crucial issue in experimental observation of QAHE in graphene [9]. Furthermore, in realistic systems, the effect of staggered sublattice potential naturally vanishes due
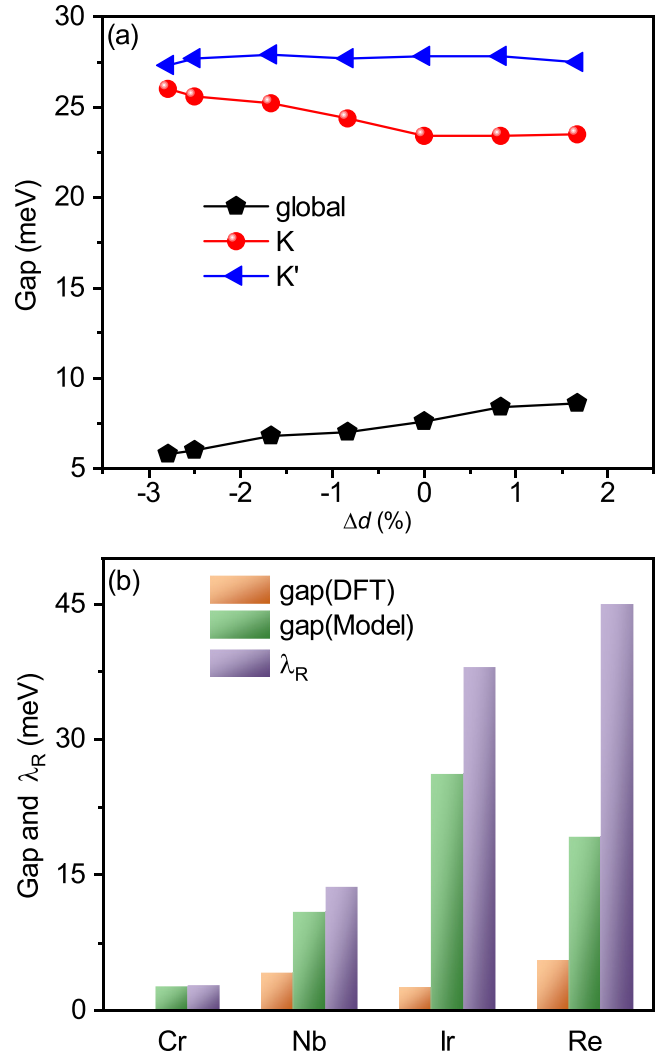
to the absence of periodicity, leading to the increase of global band gap to be around 19.5 meV (see Fig. S7).

VI. TUNABILITY OF TRANSITION-METAL-INTERCALATED SYSTEMS

From the above analysis, we know that although the local gap of each valley is sufficiently large, the global gap is determined by the band-gap alignment of the two valleys. One effective approach to tune the band gap is to apply external stress. As displayed in Fig. 4(a), the global band gap of Re-intercalated graphene/CrI$_3$ gradually increases (decreases) when applying tensile (compressive) strain, while the local gap of valleys K and K' still maintains a large value (>20 meV).

Moreover, we comprehensively study the electronic properties of $3d$, $4d$, $5d$ transition-metal intercalation in graphene/CrI$_3$ systems (see Secs. IX and X in the

Supplemental Material). We find that the system intercalated with Cr, Nb, Ir, Re demonstrates topological nontrivial properties. As displayed in Fig. 4(b) for the four types of intercalations, the global gaps from the first-principles calculations (orange bar) are small (gapless for Cr) and can be remarkably enhanced in the absence of staggered sublattice potential (green bar). The fitted Rashba SOC strength increases from Cr ($3d$) to Nb ($4d$), and to Ir and Re ($5d$). Therefore, Ir- and Re-intercalated graphene/CrI$_3$ are two preferred systems to realize large-gap QAHE due to the formation of strong Rashba SOC.

VII. SUMMARY

We have demonstrated that high-temperature QAHE can be realized in $5d$-intercalated graphene-based heterostructures due to the formation of strong Rashba SOC. Taking CrI$_3$ as an example, we find that the Re-intercalated graphene/CrI$_3$ system harbors large local gaps over 20 meV and a global band gap of 5.5 meV exhibiting the QAHE with a Chern number of $\mathcal{C} = -2$. By constructing an effective model, we show that the Rashba SOC approaches about 45 meV, which is over 30 times larger than that in graphene/BiFeO$_3$ [12]. The limited global band gap by the unaligned local gaps of valleys K and K' is attributed to the presence of staggered sublattice potential and intrinsic SOC. In realistic systems with large-scale random intercalation, the random distribution

of sublattice potentials leads to the formation of an enhanced global gap of 19.5 meV. We further show that applying tensile strain can increase the bulk gap whereas preserve the local gap at valleys K and K'. Finally, we find that Re and Ir are two preferred elements to realize QAHE in intercalated graphene/CrI$_3$ among the transition metals.

Experimentally, various graphene-based van der Waals heterostructures can be successfully fabricated [40–44], particularly for graphene/CrI$_3$ heterostructures [42–44]. And different transition-metal-intercalated graphene systems have been experimentally realized [19,20,25,45,46]. Therefore, our work paves a practical way to realize the QAHE in graphene-based system and may stimulate more theoretical and experimental explorations to search more suitable substrates and intercalated elements in graphene.

[1] F. D. M. Haldane, Phys. Rev. Lett. **61**, 2015 (1988).

[2] Y. Ren, Z. Qiao, and Q. Niu, Rep. Prog. Phys. **79**, 066501 (2016).

[3] C.-X. Liu, S.-C. Zhang, and X.-L. Qi, Annu. Rev. Condens. Matter Phys. **7**, 301 (2016).

[4] R. Yu, W. Zhang, H.-J. Zhang, S.-C. Zhang, X. Dai, and Z. Fang, Science **329**, 61 (2010).

[5] Z. Qiao, S. A. Yang, W. Feng, W.-K. Tse, J. Ding, Y. Yao, J. Wang, and Q. Niu, Phys. Rev. B **82**, 161414(R) (2010).

[6] C.-Z. Chang, J. Zhang, X. Feng, J. Shen, Z. Zhang, M. Guo, K. Li, Y. Ou, P. Wei, L. Wang, Z. Ji, Y. Feng, S. Ji, X. Chen, J. Jia, X. Dai, Z. Fang, S.-C. Zhang, K. He, and Y. Wang *et al.*, Science **340**, 167 (2013).

[7] Y. Deng, Y. Yu, M. Z. Shi, J. Wang, X. H. Chen, and Y. Zhang, Science **367**, 895 (2020).

[8] Z. Wang, C. Tang, R. Sachs, Y. Barlas, and J. Shi, Phys. Rev. Lett. **114**, 016603 (2015).

[9] C. Tang, B. Cheng, M. Aldosary, Z. Wang, Z. Jiang, K. Watanabe, T. Taniguchi, M. Bockrath, and J. Shi, APL Mater. **6**, 026401 (2018).

[10] J. Ding, Z. Qiao, W. Feng, Y. Yao, and Q. Niu, Phys. Rev. B **84**, 195444 (2011).

[11] H. Jiang, Z. Qiao, H. Liu, J. Shi, and Q. Niu, Phys. Rev. Lett. **109**, 116803 (2012).

[12] Z. Qiao, W. Ren, H. Chen, L. Bellaiche, Z. Zhang, A. H. MacDonald, and Q. Niu, Phys. Rev. Lett. **112**, 116404 (2014).

[13] J. Zhang, B. Zhao, Y. Yao, and Z. Yang, Phys. Rev. B **92**, 165418 (2015).

[14] J. Zhang, B. Zhao, T. Zhou, Y. Xue, C. Ma, and Z. Yang, Phys. Rev. B **97**, 085401 (2018).

[15] Q. Cui, J. Liang, B. Yang, Z. Wang, P. Li, P. Cui, and H. Yang, Phys. Rev. B **101**, 214439 (2020).

[16] P. Högl, T. Frank, K. Zollner, D. Kochan, M. Gmitra, and J. Fabian, Phys. Rev. Lett. **124**, 136403 (2020).

[17] H.-D. Song, P.-F. Zhu, J. Fang, Z. Zhou, H. Yang, K. Wang, J. Li, D. Yu, Z. Wei, and Z.-M. Liao, Phys. Rev. B **103**, 125304 (2021).

[18] X. Deng, S. Qi, Y. Han, K. Zhang, X. Xu, and Z. Qiao, Phys. Rev. B **95**, 121410(R) (2017).

[19] T. Gao, Y. Gao, C. Chang, Y. Chen, M. Liu, S. Xie, K. He, X. Ma, Y. Zhang, and Z. Liu, ACS Nano **6**, 6562 (2012).

[20] E. C. T. O'Farrell, J. Y. Tan, Y. Yeo, G. K. W. Koon, B. Özyilmaz, K. Watanabe, and T. Taniguchi, Phys. Rev. Lett. **117**, 076603 (2016).

[21] Y. Li, P. Chen, G. Zhou, J. Li, J. Wu, B.-L. Gu, S. B. Zhang, and W. Duan, Phys. Rev. Lett. **109**, 206802 (2012).

[22] Y. Li, D. West, H. Huang, J. Li, S. B. Zhang, and W. Duan, Phys. Rev. B **92**, 201403(R).

[23] Y. Li, P. Tang, P. Chen, J. Wu, B.-L. Gu, Y. Fang, S. B. Zhang, and W. Duan, Phys. Rev. B **87**, 245127 (2013).

[24] I. I. Klimovskikh, M. M. Otrokov, V. Yu. Voroshnin, D. Sostina, L. Petaccia, G. Di Santo, S. Thakur, E. V. Chulkov, and A. M. Shikin, ACS Nano **11**, 368 (2017).

[25] D. Marchenko, A. Varykhalov, M. R. Scholz, G. Bihlmayer, E. I. Rashba, A. G. Rybkin, A. M. Shikin, and O. Rader, Nat. Commun. **3**, 1232 (2012).

[26] A. M. Shikin, A. G. Rybkin, D. Marchenko, A. A. Rybkina, M. R. Scholz, O. Rader, and A. Varykhalov, New J. Phys. **15**, 013016 (2013).

[27] M. Krivenkov, E. Golias, D. Marchenko, J. Sanchez-Barriga, G. Bihlmayer, O. Rader, and A. Varykhalov, 2D Mater. **4**, 035010 (2017).

[28] K. Ji, J. Han, A. Hirata, T. Fujita, Y. Shen, S. Ning, P. Liu, H. Kashani, Y. Tian, Y. Ito, J. Fujita, and Y. Oyama, Nat. Commun. **10**, 275 (2019).

[29] J. Han, D. Kang, and J. Dai, RSC Adv. **8**, 19732 (2018).

[30] C. Gong, L. Li, Z. Li, H. Ji, A. Stern, Y. Xia, T. Cao, W. Bao, C. Wang, Y. Wang, Z. Q. Qiu, R. J. Cava, Steven G. Louie, J. Xia, and X. Zhang, Nature (London) **546**, 265 (2017).

[31] B. Huang, G. Clark, E. Navarro-Moratalla, D. R. Klein, R. Cheng, K. L. Seyler, D. Zhong, E. Schmidgall, M. A. McGuire, D. H. Cobden, W. Yao, D. Xiao, P. Jarillo-Herrero, and X. Xu, Nature (London) **546**, 270 (2017).

[32] M. Gibertini, M. Koperski, A. F. Morpurgo, and K. S. Novoselov, Nat. Nanotechnol. **14**, 408 (2019).

[33] B. Huang, M. A. McGuire, A. F. May, D. Xiao, P. Jarillo-Herrero, and X. Xu, Nat. Mater. **19**, 1276 (2020).

[34] P. E. Blöchl, Phys. Rev. B **50**, 17953 (1994).

[35] G. Kresse and J. Furthmuller, Phys. Rev. B **54**, 11169 (1996).

[36] G. Kresse and D. Joubert, Phys. Rev. B **59**, 1758 (1999).

[37] See Supplemental Material at http://link.aps.org/supplemental/10.1103/PhysRevB.107.205412 for the calculation methods; total energy difference of different configurations of Re-intercalated graphene/CrI_3; the interlayer distance variation and band structures of $5d$-intercalated graphene/CrI_3 systems; spin density, charge density difference, and orbital-resolved density of states of Re-intercalated graphene/CrI_3; Curie temperature estimation; electronic properties of Re-graphene without CrI_3; phase diagram of band gaps from low-energy model; atomic distance and band structures of $3d$- and $4d$-intercalated graphene/CrI_3 heterostructures; the influence of random intercalation on the band gap of the Re-intercalated graphene/CrI_3 system. The Supplemental Material also contains Refs. [47–54].

[38] J. Hu, J. Alicea, R. Wu, and M. Franz, Phys. Rev. Lett. **109**, 266801 (2012).

[39] H. Zhang, C. Lazo, S. Blügel, S. Heinze, and Y. Mokrousov, Phys. Rev. Lett. **108**, 056802 (2012).

[40] B. Karpiak, A. W. Cummings, K. Zollner, M. Vila, D. Khokhriakov, A. Md Hoque, A. Dankert, P. Svedlindh, J. Fabian, S. Roche, and S. P. Dash, 2D Mater. **7**, 015026 (2020).

[41] Y. Wu II, G. Yin, L. Pan, A. J. Grutter, Q. Pan, A. Lee, D. A. Gilbert, J. A. Borchers, W. Ratcliff II, A. Li, X.-D. Han, and K. L. Wang, Nat. Electron. **3**, 604 (2020).

[42] Z. Qiu, M. Holwill, T. Olsen, P. Lyu, J. Li, H. Fang, H. Yang, M. Kashchenko, K. S. Novoselov, and J. Lu, Nat. Commun. **12**, 70 (2021).

[43] C.-C. Tseng, T. Song, Q. Jiang, Z. Lin, C. Wang, J. Suh, K. Watanabe, T. Taniguchi, M. A. McGuire, D. Xiao, J.-H. Chu, D. H. Cobden, X. Xu, and M. Yankowitz, Nano Lett. **22**, 8495 (2022).

[44] S. Jiang, L. Li, Z. Wang, J. Shan, and K. F. Mak, Nat. Electron. **2**, 159 (2019).

[45] I. S. Sokolov, D. V. Averyanov, O. E. Parfenov, I. A. Karateev, A. N. Taldenkov, A. M. Tokmacheva, and V. G. Storchak, Mater. Horiz. **7**, 1372 (2020).

[46] S. Schumacher, F. Huttmann, M. Petrovic, C. Witt, D. F. Förster, C. Vo-Van, J. Coraux, A. J. Martínez-Galera, V. Sessi, I. Vergara, R. Rückamp, M. Grüninger, N. Schleheck, F. M. zu Heringdorf, P. Ohresser, M. Kralj, T. O. Wehling, and T. Michely, Phys. Rev. B **90**, 235437 (2014).

[47] D. J. Thouless, M. Kohmoto, M. P. Nightingale, and M. den Nijs, Phys. Rev. Lett. **49**, 405 (1982).

[48] V. I. Anisimov, J. Zaanen, and O. K. Anderson, Phys. Rev. B **44**, 943 (1991).

[49] A. A. Mostofi, J. R. Yates, Y.-S. Lee, I. Souza, D. Vanderbilt, and N. Marzari, Comput. Phys. Commun. **178**, 685 (2008).

[50] J. P. Perdew, K. Burke, and M. Ernzerhof, Phys. Rev. Lett. **77**, 3865 (1996).

[51] S. Qi, Z. Liu, M. Chang, R. Gao, Y. Han, and Z. Qiao, Phys. Rev. B **101**, 241407(R) (2020).

[52] S. Grimme, J. Antony, S. Ehrlich, and H. Krieg, J. Chem. Phys. **132**, 154104 (2010).

[53] S. L. Dudarev, G. A. Botton, S. Y. Savrasov, C. J. Humphreys, and A. P. Sutton, Phys. Rev. B **57**, 1505 (1998).

[54] S. Grimme, S. Ehrlich, and L. Goerigk, J. Comput. Chem. **32**, 1456 (2011).